Title

PERTURBED ANGULAR CORRELATION OP 111mCd IN ANTIFERROMAGENETIC MbF2, FeF2, CoF2 AND NiF2

Authors

Rinneberg, H.H.
Shirley, D.A.

Publication Date

1974-04-01

Submitted to Physical Review B

LBL-2398
Preprint

PERTURBED ANGULAR CORRELATION OF ^{111m}Cd IN ANTIFERROMAGNETIC MnF_2, FeF_2, CoF_2 AND NiF2

H. H. Rinneberg and D. A. Shirley

April 1974

Prepared for the U. S. Atomic Energy Commission
under Contract W-7405-ENG-48

DISCLAIMER

PERTURBED ANGULAR CORRELATION OF ^{111m}Cd IN ANTIFERROMAGNETIC MnF_2, FeF_2, CoF_2 and NiF_2*

H. H. Rinneberg and D. A. Shirley

Department of Chemistry and
Lawrence Berkeley Laboratory
University of California
Berkeley, California 94720

April 1974

ABSTRACT

The time differential perturbed angular correlation (PAC) of ^{111m}Cd doped into antiferromagnetic MnF_2, FeF_2, CoF_2 and NiF_2 has been observed. The perturbation is caused by a combined electric quadrupole and magnetic dipole interaction. The PAC spectra are analyzed using autocorrelation-Fourier transformation techniques. The following quadrupole coupling parameters and internal fields have been observed (4°K) MnF_2: $\nu_Q = 16.7 \pm 0.2$ MHz, $\eta = 0.05 \pm 0.02$, $H_{int} = 33.1 \pm 0.8$ kOe; FeF_2: $\nu_Q = 21.6 \pm 0.3$ MHz, $\eta = 0.49 \pm 0.02$, $H_{int} = 38.7 \pm 0.8$ kOe; CoF_2: $\nu_Q = 17.7 \pm 0.3$ MHz, $\eta = 0.0 \pm 0.02$, $H_{int} = 15.8 \pm 0.8$ kOe; NiF_2: $\nu_Q = 16.5 \pm 0.3$ MHz, $\eta = 0.1 \pm 0.08$ $H_{int} = 23.5 \pm 0.8$ kOe. The internal fields are perpendicular to the z-axis z_{FG} of the field gradient tensor for MnF_2, FeF_2 and CoF_2, parallel to y_{FG} in MnF_2 and pointing along x_{FG} in FeF_2. In NiF_2 the internal field is found in the z_{FG}, x_{FG} plane tilted by approximately 48 ± 5° against the z_{FG} axis. The hyperfine fields are caused by unpaired spin density transferred into Cd s orbitals from 2 nearest and 8 next nearest magnetic ions belonging to two different sublattices. The internal fields are compared with those found in the corresponding perovskites $KNiF_3$, $KCoF_3$, $KFeF_3$ and $RbMnF_3$.

I. INTRODUCTION

In recent years the perturbed angular correlation[1] (PAC) of γ rays has been increasingly applied to investigate the interaction of a nucleus with its chemical environment. Using this technique, Haas[2] et al. have made a comprehensive study of nuclear quadrupole interactions. In a preceding letter,[3] we reported the PAC of ^{111m}Cd doped as a dilute impurity into the cubic antiferromagnets $KNiF_3$, $KCoF_3$, and $RbMnF_3$, demonstrating how the measured hyperfine fields can be used to obtain new estimates for the spin density parameters f_σ of the cobalt-fluorine and manganese-fluorine bonds.

The experiments described in this paper are part of a continuing effort to understand the transfer of spin density in inorganic magnetically ordered insulators using Cd^{2+} as a probe, a problem closely related to superexchange. Because of the lower site symmetry the angular correlation of ^{111m}Cd in antiferromagnetic MnF_2, FeF_2, CoF_2 and NiF_2 is perturbed by a magnetic dipole and an electric quadrupole interaction. The PAC spectra reported here are some of the best examples for combined interactions.

In Sec. II we give some experimental details. Section III deals with the spectral analysis using autocorrelation-Fourier transformation techniques. In Sec. IV we discuss the individual paths involved in the transfer of spin density.

II. EXPERIMENTAL

The ^{111m}Cd was obtained by neutron irradiation of ^{110}CdO. Subsequently the oxide was converted to the fluoride and then heated with the corresponding anhydrous transition metal fluoride in a Pt crucible. After cooling the melts were ground up in a mortar, to obtain a randomly oriented source. Typically the transition metal fluorides were doped with 0.1 mole % Cd.

Zone refined MnF_2 and CoF_2 were purchased from Atomergic Chemicals Co., New York. Anhydrous FeF_2 was prepared by passing HF gas over high purity iron at 1050-1100 °C. The product was zone refined in a sealed Pt crucible. NiF_2 was obtained by heating anhydrous $NiCl_2$ in a stream of fluorine at 450°C. It was sublimed subsequently in a stream of HF at 1200°C.

For MnF_2, FeF_2 and CoF_2 the spectra were taken with a conventional fast-slow four detector setup.[2] For NiF_2/Cd we used an eight detector spectrometer, where each counter could be used as a START and a STOP detector. A total of eight 180° and eight 90° spectra were taken simultaneously. As described earlier,[2] the perturbation factor $A_{22}G_{22}(t)$ can be directly obtained by combining corresponding 180° and 90° spectra.

III. SPECTRA ANALYSIS

The divalent fluorides MnF_2 ($T_N = 67.4°K$), FeF_2 ($T_N = 78.1°K$), CoF_2 ($T_N = 37.7°K$) and NiF_2 ($T_N = 73.2°K$) have the rutile structure (D_{4h}^{14}) shown in Fig. 1. There are two crystallographically equivalent cations per unit cell, related to each other by a 90° rotation. Cd^{2+} enters substitutionally for a transition metal ion, e.g. at the center of the cube. It is surrounded by a distorted octahedron of fluoride ions. Four anions at the corners of a rectangle in the (110) plane are equivalent (Me-F bond type I), while the two remaining F^- ions above and below the plane have a slightly shorter Me-F distance (Me-F bond type II). Because of the point symmetry at the metal site (D_{2h}) the orientation of the field gradient tensor, produced by the crystalline surroundings at the Cd nucleus, is fixed with the principal axes pointing along [110], [$\bar{1}$10], and [001].

In the antiferromagnetic state there are two interpenetrating sublattices. For MnF_2, FeF_2 and CoF_2 (Fig. 1a) the spins point along the c-axis. Hence the hyperfine field at the Cd nucleus is parallel to [001], that is, one of the axes of the field gradient tensor. Because of symmetry the combined magnetic dipole and electric quadrupole interaction is the same for cadmium ions entering substitutionally at the center and the corners of the cube.

The spin structure of NiF_2 (Fig. 1b) is more complicated. The spins are perpendicular to the c-axis, with the spin axis along [100] or [010]. It is well known that a slight canting of the spins occurs, giving rise to a small ferromagnetic component. There are four equivalent magnetic domains (Fig. 2).

However, as can be seen from Fig. 2, the orientation of the internal field of the cadmium nucleus relative to the field gradient tensor is effectively the same for the four domains, if we neglect the small rhombic lattice distortion associated with the magnetic transition. Under this assumption cadmium ions entering substitutionally at the center and the corners of the cube are subject to the same combined magnetic dipole and electric quadrupole interaction.

The angular correlation of the well known γ-γ cascade of ^{111m}Cd into antiferromagnetic MnF_2, FeF_2, CoF_2 and NiF_2 is therefore perturbed by the combined interaction[4] of the Cd nucleus in the intermediate 247 keV state ($I = 5/2$, $\tau_N = 84$ nsec)

$$\mathcal{H} = -\gamma\hbar \vec{H}_{int} \cdot \vec{I} + \frac{e^2qQ}{4I(2I-1)} \{3I_z^2 - I(I+1) + \eta(I_x^2 - I_y^2)\} \quad .$$

The components of $\vec{I}$ refer to the principal axes of the field gradient tensor, $\frac{e^2qQ}{h}$ is the quadrupole coupling constant, η the asymmetry parameter, and H_{int} is the internal magnetic field at the Cd nucleus. For a polycrystalline sample; that is, a unique but randomly oriented interaction, the angular correlation is given by[1]

$$W(\theta,t) = 1 + A_{22}G_{22}(t)\ P_2(\cos\theta)$$

where $G_{22}(t) = G_{22}^{*}(t)$ is the perturbation factor

$$G_{22}(t) = \sum_{N=-2}^{+2} \sum_{n_1,n_2} \sum_{m_1 m_2} (-1)^{2I+m_1+m_2} \exp\left(-\frac{i}{\hbar}(E_{n_1} - E_{n_2})t\right)$$

$$\times \begin{pmatrix} I & I & 2 \\ m_1' & -m_1 & N \end{pmatrix} \begin{pmatrix} I & I & 2 \\ m_2' & -m_2 & N \end{pmatrix} \langle n_1|m_2\rangle^{*} \langle n_1|m_1\rangle \langle n_2|m_2'\rangle \langle n_2|m_1'\rangle^{*} \quad . \quad (1)$$

Here $|m_1\rangle$, $|m_1'\rangle$, $|m_2\rangle$, $|m_2'\rangle$ are eigenfunctions of I_z quantized along the z-axis of the field gradient tensor, $|n_1\rangle$, $|n_2\rangle$ are eigenvectors of $\mathcal{H}$ belonging to the eigenvalues E_{n_1} and E_{n_2} respectively. In the paramagnetic state ($H_{int} = 0$) and for an axially symmetric quadrupole interaction ($\eta = 0$), the expression can be written as[1]

$$G_{22}(t) = \frac{1}{5}\left\{1 + \frac{13}{7}\cos(2\pi\,\nu_Q t) + \frac{10}{7}\cos(4\pi\,\nu_Q t) + \frac{5}{7}\cos(6\pi\,\nu_Q t)\right\} \quad (2)$$

with

$$\nu_Q = \frac{3e^2qQ}{h2I(2I-1)} \quad .$$

The time differential perturbed angular correlation spectra of ^{111m}Cd doped into MnF_2, FeF_2, CoF_2, and NiF_2 are shown in Figs. 3 and 4 for temperatures below and above their Néel points. The spectrum obtained for MnF_2 in the paramagnetic state (77°K) shows almost exactly the periodic variation expected from Eq. (2). Therefore approximate values for ν_Q and η ($\eta \approx 0$) are easily obtained, which can be improved by a least-squares fit using for $G_{22}(t)$ the general expression (1).

For paramagnetic FeF_2 ($T = 90°K$, $H_{int} = 0$) the observed PAC spectrum is no longer periodic. Since ν_Q essentially determines the time scale, the specific form of $G_{22}(t)$ depends only on the asymmetry parameter $0 \leqslant \eta \leqslant 1$, which is easily found by trial and error. However in the antiferromagnetic state, where more parameters have to be determined, this method becomes increasingly difficult and tedious. Clearly, the Fourier components $(E_{n_1} - E_{n_2})/h$ of the perturbation factor $G_{22}(t)$, which are differences of the eigenvalues of the hamiltonian $\mathcal{H}$, are needed to estimate these parameters. In principle the Fourier components can be obtained by a discrete Fourier transformation of the experimental spectra. However, whereas $G_{22}(t)$ contains three frequencies in the case of an axially symmetric quadrupole coupling, up to fifteen Fourier components have to be determined for the combined interaction. Since the area under the frequency spectrum remains constant (=1) the increased splitting leads to a considerable drop in amplitude, which makes it difficult or impossible to discriminate the Fourier components from the noise associated with the statistical fluctuations of the time differential PAC spectra.

These difficulties can be overcome by using the autocorrelation function of the perturbation factor, rather than $G_{22}(t)$ itself. The autocorrelation function $C_f(\tau)$ of the time dependent function $f(t)$ is defined as the ensemble average

$$C_f(\tau) = \overline{f(t) \cdot f(t + \tau)} \quad ,$$

where a stationary ensemble has been assumed. For most applications the ensemble average can be replaced by a time average

$$C_f(\tau) = \lim_{T \to \infty} \frac{1}{T} \int_{-T/2}^{+T/2} f(t) \cdot f(t + \tau)\, dt \quad .$$

It is well known[5] that the Fourier transform of the autocorrelation function (multiplied by $1/2\pi$) is the average power spectral density $W(\omega)$ associated with the time function $f(t)$

$$W_f(\omega) = \frac{1}{2\pi} \int_{-\infty}^{+\infty} C_f(\tau)\, e^{-i\omega\tau}\, d\tau$$

$$W_f(\omega) = \lim_{T \to \infty} \frac{1}{T} \frac{1}{2\pi} \overline{\left| \int_{-T/2}^{+T/2} f(t)\, e^{-i\omega t}\, dt \right|^2} \quad ,$$

where the average is taken over the ensemble. If the time function $f(t) = s(t) + n(t)$ is the sum of a signal and of noise, with zero time (ensemble) averages, the autocorrelation function can be written as

$$C(\tau) = \overline{f(t) \cdot f(t+\tau)} + \overline{f(t)} \cdot \overline{n(t+\tau)} + \overline{n(t)} \cdot \overline{f(t+\tau)} + \overline{n(t) \cdot n(t+\tau)}$$

$$C(\tau) = C_s(\tau) + C_n(\tau) \quad .$$

Since signal and noise are incoherent, the cross terms drop out and the autocorrelation function is the sum of the corresponding functions for signal and noise. Hence the Fourier transform of the autocorrelation function is (apart from the factor $1/2\pi$) the sum of the average power spectral densities of signal and noise respectively. This can also be seen immediately from the expression for $W(\omega)$ itself. By contrast, these cross terms are contained in the power spectral density $P(\omega) = \lim_{T \to \infty} \frac{1}{T} \frac{1}{2\pi} \left| \int_{-T/2}^{+T/2} f(t) e^{-i\omega t}\, dt \right|^2$ which is directly obtained from the Fourier transform $F(\omega)$ of $f(t)$ itself. Therefore using the auto-correlation function of the perturbation factor $G_{22}(t)$, which represents the time information in a smoothed form, leads to an average power density spectrum

with a greatly improved signal/noise ratio. Recently several authors[6,7,8] have used the Fourier transform $F(\omega)$ of the perturbation factor $G_{22}(t)$ or the power spectral density $P(\omega)$ derived from it to analyze pure quadrupole PAC spectra. However, the use of autocorrelation functions which was originally introduced by Matthias et al.[9] and subsequently applied by Rao et al.[10] to time differential PAC spectra perturbed by a pure magnetic dipole interaction is far superior and necessary to analyze more complicated spectra reliably.

In the following we discuss some of the computational details. Since the coincidence spectrum $N(t,\theta) = N_o e^{-t/\tau_N} (1 + A_{22} G_{22}(t) P_2(\cos\theta)) + N_r$ is observed only for a certain period of time, the perturbation factor $G_{22}(t)$ is obtained experimentally (in digital form) within a finite time interval. For times $t > t_{max}$, for which the number of true coincidences is smaller than the background due to random events $N_o e^{-t/\tau_N} < N_r$, the statistical error increases significantly as can be seen from Figs. 3 and 4. These data points carry little signal information and are dropped. In order to obtain a maximum length for the usable portion of $G_{22}(t)$, and hence optimum frequency resolution, the background due to random coincidences should be kept as low as possible.

Initially the data obtained are smoothed within the time interval $0 \leq t \leq t_{max}$ according to $G'_{22}(i) = 0.5\, G_{22}(i) + 0.25\, G_{22}(i-1) + 0.25\, G_{22}(i+1)$. Here the index i is the channel number. Furthermore, since the statistical error of the experimental perturbation factor is known, $G_{22}(t)$ already represents an average rather than a single member of an ensemble. Hence the discrete values of $G'_{22}(t)$ are weighed according to the inverse $g(t)$ of the relative error $\frac{\Delta N(t)}{N(t)}$. For the time interval $0 \leq t \leq t_{max}$, $g(t) \sim e^{-t/2\tau_N}$ holds to a good approximation. In order to avoid side bands, this function is tapered off to zero for times $t \approx t_{max}$. With the values $G''_{22}(t) = e^{-t/2\tau_N} \cdot G'_{22}(t)$ thus obtained the autocorrelation function $C(\tau)$

is calculated for time lags $0 \leqslant \tau \leqslant \tau_{max} = t_{max}$. Subsequently the discrete values of $C(\tau)$ obtained are reflected at $\tau = 0$ so that $C(-\tau) = C(+\tau)$. The average power spectral density $W(\omega)$ is then calculated by a discrete (fast)[11] Fourier transformation of the autocorrelation function $C(\tau)$. However, in order to suppress side bands, $C(\tau)$ is multiplied by the time window[5] $D(\tau) = 0.54 + 0.46 \cos(\pi \cdot \tau/\tau_{max})$ before transformation. In order to increase the number of points calculated and thus to improve the spectral appearance and definition, additional zeroes are added to $C(\tau)$ outside the interval $-\tau_{max} \leqslant \tau \leqslant \tau_{max}$ to create an apparently longer signal. This of course does not affect the (physical) frequency resolution.

In this way we obtain from the experimental time differential PAC spectra (Figs. 3 and 4) the experimental average power spectral density functions W^{exp} shown in Figs. 5 and 6 for MnF_2, FeF_2, CoF_2, and NiF_2 (dotted lines). Since the natural line width associated with the γ-γ cascade of ^{111m}Cd, $\Delta\nu = (\pi\tau_N)^{-1}$, is about 2.5 MHz, the individual Fourier components overlap heavily. Assuming certain values for ν_Q, η, and $\vec{H}_{int}$, the perturbation factor $G_{22}(t)$ is calculated. Using these theoretical estimates instead of the measured values for $G_{22}(t)$, a theoretical estimate of the average power spectral density W^{calc} can be made, following exactly the same procedure as described above. Comparing W^{calc} with W^{exp} approximate values for the unknown parameters in the hamiltonian are easily found. They can be improved by a least-squares fit of W^{calc} and W^{exp} in the frequency or by a fit of G_{22}^{calc} and G_{22}^{exp} in the time domain. Good agreement was obtained between the results of a minimization in frequency space and time space. The solid curves in Figs. 5,6 and 3,4 represent the calculated average power spectral density W^{calc} and perturbation factor G_{22}^{calc} respectively.

IV. DISCUSSION

As can be seen from Table I, the quadrupole coupling constant ν_Q is rather similar for Cd^{2+} doped into MnF_2, FeF_2, CoF_2, and NiF_2. The asymmetry parameter η is surprisingly small for MnF_2/Cd, CoF_2/Cd, and NiF_2/Cd. In FeF_2 on the other hand, where the difference between the lengths of the transition metal-fluorine bonds (2.122 Å type I, 1.993, type II) is largest, an asymmetry parameter $\eta \approx 0.5$ is found. Since the quadrupole coupling constants ν_Q and the Larmor frequencies corresponding to the observed internal fields are of the same order of magnitude, the energy levels of the hamiltonian $\mathcal{H}$ are strongly mixed, depending on the relative orientation of the internal magnetic field and the field gradient tensor. In this way the internal field was found in MnF_2, FeF_2, and CoF_2 to be perpendicular to the z-axis z_{FG} of the field gradient tensor, pointing along x_{FG} in FeF_2 and y_{FG} in MnF_2. Within our accuracy no change in the quadrupole coupling due to the magnetic transition was observed for MnF_2/Cd, FeF_2/Cd, and CoF_2/Cd.

Because of the different spin structure the internal field at the cadmium nucleus in NiF_2 is perpendicular to the y_{FG} axis (c-axis). Therefore besides ν_Q, H_{int} and η the angle θ between the internal field and the z-axis z_{FG} of the field gradient tensor has to be determined. If one neglects the small tilt ($\sim 1.3°$) of the spins from the [100] or [010] direction towards [110], the angle θ would be 45°. Whereas ν_Q and H_{int} are rather insensitive towards the value chosen for θ of course it is strongly correlated with the asymmetry parameter η. Assuming $\theta = 45°$ a reasonable fit of the experimental data is obtained for $\eta \approx 0.2$, whereas $\eta = 0.06 \pm 0.04$ is found in the paramagnetic state. A slightly better agreement between experimental and calculated values of the perturbation factor $A_{22}G_{22}(t)$ is found for $\theta = 51°$ and $\eta = 0.05$. The

error limits for θ and η quoted in Table I reflect the strong correlation between these two parameters. If one assumes that the rhombic lattice distortion, associated with the magnetic transition in NiF_2 is too small to cause an observable change in the quadrupole coupling, then the better fit obtained for $\theta = 51°$ using the quadrupole coupling parameters found in the paramagnetic state reflects the influence of the spin canting on the time differential PAC spectrum. Lattice distortions, caused by a magnetic transition are generally small. As reported earlier[3] within our accuracy no quadrupole coupling was found in antiferromagnetic $KCoF_3$ where at the Néel point a tetragonal distortion of the cubic perovskite occurs.

The internal fields (Table I) found in MnF_2/Cd, FeF_2/Cd, CoF_2/Cd, and NiF_2/Cd at 4°K are rather similar. For comparison we include in Table I the hyperfine fields at the Cd nucleus doped into the antiferromagnetic perovskites $RbMnF_3$, $KFeF_3$, $KCoF_3$, and $KNiF_3$. Because of the lower site symmetry, the internal fields found in the divalent fluorides MeF_2 should be corrected for dipolar fields, which generally amount to a few kOe. Jones et al.[12] reported for the dipolar field at a manganese site in antiferromagnetic MnF_2 a value of $H_{dip} = 5.8$ kOe. Although we do not know the relative sign of the hyperfine and dipolar field, it can be seen from Table I that the hyperfine fields in the divalent fluorides are considerably smaller than those in the corresponding perovskites.

Recently[13] the hyperfine fields have been calculated for $KNiF_3$/Cd and NiO/Cd. Cd^{2+} is surrounded by six magnetic ions belonging to the same sublattice in the antiferromagnetic state. Assuming spin density only to be transferred into the outermost filled (4s) and empty (5s) shells of Cd^{2+}, good agreement was obtained with the experimentally observed fields. It was found

that the major contribution to the hyperfine field was caused by an overlap effect of the spin polarized $2p_\sigma$ orbital of $F^-(0^{2-})$ and the 4s orbital of Cd^{2+}. Because of the electronic ground state of Ni^{2+} in an octahedral crystal field only σ bonding had to be considered. In this way the contribution of a single path $Ni^{2+} - F^-(0^{2-}) - Cd^{2+}$ to the hyperfine field was found to be approximately

$$H_{int} \approx - \frac{8\pi}{3} \beta_e |\psi_{4s}(0)|^2 \frac{\langle S \rangle}{S} (\sqrt{f_\sigma} \langle p_\sigma | 4s \rangle - \sqrt{f_s} \langle 2s | 4s \rangle)^2 \quad . \qquad (3)$$

More generally, since spin transfer occurs in the perovskites along linear bonds $Me^{2+} - F^- - Cd^{2+}$ only σ bonding contributes to the hyperfine field in $RbMnF_3/Cd$, $KCoF_3/Cd$, and $KFeF_3/Cd$, although some of the π-bonding t_{2g} orbitals are half occupied.

For the rutile type difluorides MnF_2, FeF_2, CoF_2, and NiF_2 the situation is considerably more complicated. Cd^{2+} which enters substitutionally at the center of the cube (Fig. 1) has 2 nearest magnetic neighbors along the c-axis belonging to one and eight next nearest neighbors at the corners belonging to the other sublattice. Thus the hyperfine fields produced by the two sublattices at the Cd nucleus generally tend to cancel. As can be seen from Fig. 1, Cd^{2+} is connected to the surrounding magnetic ions by angular bonds $Cd^{2+} - F^- \diagdown Me^{2+}$. Hence transition metal-fluorine bonds (Me-F) of both σ and π character will contribute to the spin density in Cd s orbitals. Whereas the π bonding t_{2g} orbitals are half occupied in $MnF_2(d^5)$, for $Ni^{2+}(d^8)$ to a good approximation there are no unpaired electrons in these orbitals. Therefore in MnF_2, FeF_2, CoF_2, and NiF_2 different amounts of unpaired spin density will be transferred from t_{2g} orbitals into Cd s shells. However as can be seen from Table I for the divalent fluorides the internal fields at the Cd nucleus are surprisingly similar. This suggests that the transfer of spin density along transition-metal-fluorine π

bonds contributes rather little to the unpaired spin density in cadmium s orbitals. Furthermore, as will be shown below, in NiF_2/Cd because of symmetry the spin transfer from the two nearest Ni^{2+} ions belonging to one sublattice can be neglected to a good approximation. Hence in NiF_2 the hyperfine field at the cadmium nucleus is mainly caused by 8 next nearest neighbors, at the corners of the cube. Comparing the hyperfine field in $KNiF_3$/Cd (102 kOe) and the internal field in NiF_2/Cd (23.5 kOe), we see that in the perovskite $KNiF_3$ one linear bond $Ni^{2+} - F^- - Cd^{2+}$ contributes 17 kOe to the hyperfine field, whereas the spin transfer along the angular path $Ni^{2+}-F \smile Cd^{2+}$ involving a (Ni-F) σ-bond causes only a hyperfine field of approximately 3 kOe. This shows that the spin transfer along angular bonds is rather inefficient and suggests that for the remaining rutile type difluorides MnF_2, FeF_2, and CoF_2 the small hyperfine fields reflect small amounts of spin density transferred along angular bonds (of both σ and π character) rather than an almost complete cancellation of the hyperfine fields caused by the two magnetic sublattices.

In the following paragraph we discuss qualitatively the individual paths along which spin density is thought to be transferred. We chose (Fig. 1) the positive direction [100] to point to the front, the positive direction [010] to the right and [001] points to the top of the page. For each ion in the unit cell a coordinate system is assumed, with the x-axis pointing along [001]. For Cd^{2+}, which enters substitutionally at the center of the cube and its two nearest magnetic neighbors (above and below) the z-axis is taken along $[\bar{1}\bar{1}0]$. For the magnetic ions at the corners of the cube the z-axis points along $[\bar{1}10]$. The same coordinate system is used for the four fluorine ions in the (110) plane. The point symmetry at a metal site is D_{2h}, at a fluorine ion C_{2v}, prior to doping. We neglect the lowering of the symmetry due to the dopant. We neglect

the difference in the transition metal-fluorine bond length (type I and II). We take the bond angles $Cd^{2+} - F^{-} - Me^{2+}$ with the nearest and next nearest magnetic ions Me^{2+} to be 90° and 135° respectively rather than the actual values 102° and 129°. Under these assumptions the four next nearest magnetic ions in the $(\bar{1}10)$ plane contribute as much to the spin density in cadmium s orbitals as the remaining four next nearest metal ions in the (110) plane. Since the cadmium s orbitals are invariant with reflections through the mirror planes (110) and $(\bar{1}10)$ only those d orbitals of the transition metal ions with a corresponding symmetry behavior have to be considered: $|d_{z^2}\rangle$, $|d_{xz}\rangle$ (next nearest neighbors in (110)), $|d_{z^2}\rangle$, $|d_{x^2-y^2}\rangle$ (nearest neighbors). Similarly only the fluorine orbitals $2p_x$ and $2p_z$ have to be taken into account. The transfer of spin density along the c-axis from the nearest magnetic ions via the fluorine anions in the (110) plane is appreciable only for the $|d_{x^2-y^2}\rangle$ function. The $|d_{z^2}\rangle$ function of the nearest magnetic neighbors is perpendicular to the $|2p_x\rangle$ and $|2p_z\rangle$ orbitals of the bridging fluorine anions and hence a small overlap is expected. Therefore, in NiF_2, for which $|d_{z^2-y^2}\rangle$ is doubly occupied, only the eight next nearest magnetic neighbors contribute appreciably to the hyperfine field at the cadmium nucleus.

In order to compare the hyperfine fields in NiF_2/Cd and $KNiF_3$/Cd, expression (3) has to be modified for the transfer of spin density along non-linear $Ni^{2+} - F^{-} \diagdown Cd^{2+}$ bonds. The easiest way is to assume the nickel-fluorine and fluorine-cadmium bonds to be independent of each other. This assumption is closely related to the independent bond model used to interpret the ^{19}F NMR data in MnF_2 and NiF_2 and to the factorization of exchange parameters into contributions of each individual bond within a certain superexchange path, recently proposed by Newman.[16] Under this assumption, the overlap integral

$\langle p_\sigma | 4s \rangle$ in expression (3), where the p_σ function points along the nickel-fluorine bond is merely replaced by $\langle p | 4s \rangle \cos 45°$ with $|p\rangle$ along the cadmium-fluorine axis. It is well known from the ^{19}F - NMR investigations of Shulman et al.[15,17] in NiF_2 and $KNiF_3$ that the spin density parameters f_σ, f_s for the nickel-fluorine bond are about the same in the two fluorides. Neglecting the small contribution of the fluorine $|2s\rangle$ orbital to the spin transfer, one obtains for the hyperfine field at the cadmium nucleus in NiF_2/Cd: $H(NiF_2/Cd) \approx \frac{8}{6} H(KNiF_3/Cd)\cos^2 45°$. In this way a field of $H(NiF_2/Cd) \approx 68$ kOe is estimated, which is in poor agreement with the experimentally observed internal field $H_{int} \approx 24$ kOe. Therefore our experimental results in NiF_2/Cd and $KNiF_3$/Cd suggest that the transfer of spin density along angular paths cannot be estimated from that observed for 180° bonds simply by taking a reduced overlap of ligand and metal functions into account.

Although our discussion has been only qualitative, the data presented here show important differences between supertransferred hyperfine fields in the transition metal difluorides and the corresponding perovskites. A more rigorous theory of the properties of these materials should be able to account for these differences.

V. CONCLUSION

The time differential perturbed angular correlation (PAC) of ^{111m}Cd doped into antiferromagnetic MnF_2, FeF_2, CoF_2, and NiF_2 was observed. Well resolved hyperfine structure due to a magnetic dipole and electric quadrupole interaction was found in each case. The spectra were analyzed using autocorrelation-Fourier transformation techniques. The observed hyperfine fields are discussed in terms of unpaired spin density transferred into the closed Cd 4s shell along angular transition metal-fluorine-cadmium bonds.

FOOTNOTES AND REFERENCES

*Work performed under the auspices of the U. S. Atomic Energy Commission.

1. H. Frauenfelder and R. M. Steffen, in Alpha-, Beta-, and Gamma-Ray Spectroscopy, ed. by K. Siegbahn (North-Holland, 1965), Vol. 2.
2. H. Haas and D. A. Shirley, J. Chem. Phys. 58, 3339 (1973).
3. H. H. Rinneberg and D. A. Shirley, Phys. Rev. Letters 30, 1147 (1973).
4. A. Abragam, The Principles of Nuclear Magnetism (Clarendon Press, Oxford, 1961).
5. R. B. Blackman and J. W. Tukey, The Measurement of Power Spectra (Dover, New York, 1958); reprinted from Bell Tech. J. 37 (1), 185 (1958); 37 (2), 485 (1958).
6. E. Gerdau, J. Wolf, H. Winkler, and J. Braunsfurth, Proc. Roy. Soc. (London) Ser. A 311, 197 (1969).
7. P. R. Gardner and W. V. Prestwich, Can. J. Phys. 48, 1430 (1970).
8. M. Forker and J. D. Rogers, Nucl. Instr. Methods 96, 453 (1971).
9. E. Matthias and D. A. Shirley, Nucl. Instr. Methods 45, 309 (1966).
10. G. N. Rao, E. Matthias, and D. A. Shirley, Phys. Rev. 184, 325 (1969).
11. E. O. Brigham, The Fast Fourier Transform (Prentice Hall, Englewood Cliffs, New Jersey, 1973).
12. E. D. Jones and K. B. Jefferts, Phys. Rev. 135, A1277 (1964).
13. H. H. Rinneberg and D. A. Shirley, to be published.
14. R. G. Shulman and V. Jaccarino, Phys. Rev. 108, 1219 (1957).
15. R. G. Shulman, Phys. Rev. 121, 125 (1961).
16. D. J. Newman, J. Phys. C 5, 1098 (1972).
17. R. G. Shulman and S. Sugano, Phys. Rev. 130, 506 (1963).

Table I.

	ν_Q(MHz)	η	H_{int}(kOe)	
MnF_2	16.7 ± 0.2	0.05 ± 0.02	33.1 ± 0.8	$H_{int} \parallel y_{FG}$
FeF_2	21.6 ± 0.3	0.49 ± 0.02	38.7 ± 0.8	$H_{int} \parallel x_{FG}$
CoF_2	17.7 ± 0.3	0.0 ± 0.02	15.8 ± 0.8	$H_{int} \perp z_{FG}$
NiF_2	16.5 ± 0.5	0.1 ± 0.08	23.5 ± 0.8	H_{int} in x_{FG}, z_{FG} plane
				$\measuredangle H_{int}, z_{FG} = 48 \pm 5°$
$RbMnF_3$	--	--	111.4 ± 1.5	--
$KFeF_3$	--	--	∿100	--
$KCoF_3$	--	--	71.7 ± 1.5	--
$KNiF_3$	--	--	101.7 ± 1.5	--

FIGURE CAPTIONS

Fig. 1. The crystal and magnetic structure of a) antiferromagnetic MnF_2, FeF_2, and CoF_2 and b) weakly ferromagnetic NiF_2. The cadmium ion enters substitutionally e.g. at the center of the cube.

Fig. 2. For equivalent spin arrangements in weakly ferromagnetic NiF_2.

Fig. 3. Time differential PAC spectra of ^{111m}Cd doped into paramagnetic and antiferromagnetic MnF_2, FeF_2, and CoF_2.

Fig. 4. Time differential PAC spectra of ^{111m}Cd in paramagnetic and weakly ferromagnetic NiF_2.

Fig. 5. Average power spectral density of the time differential PAC spectra (dotted line) for MnF_2/Cd, FeF_2/Cd, and CoF_2/Cd. The solid curves represent a least squares fit.

Fig. 6. Average power spectral density of the time differential PAC spectrum of NiF_2/Cd at 4°K (dotted line). The solid curve represents a least squares fit.

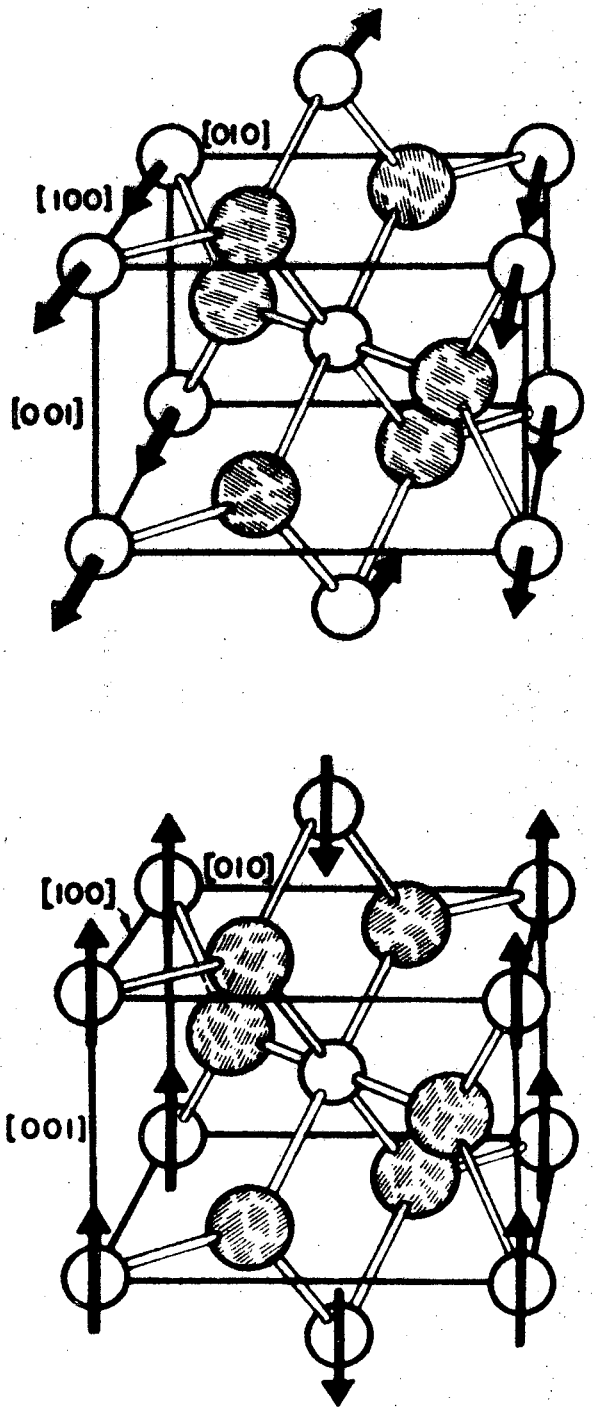

XBL744-2828A

Fig. 1

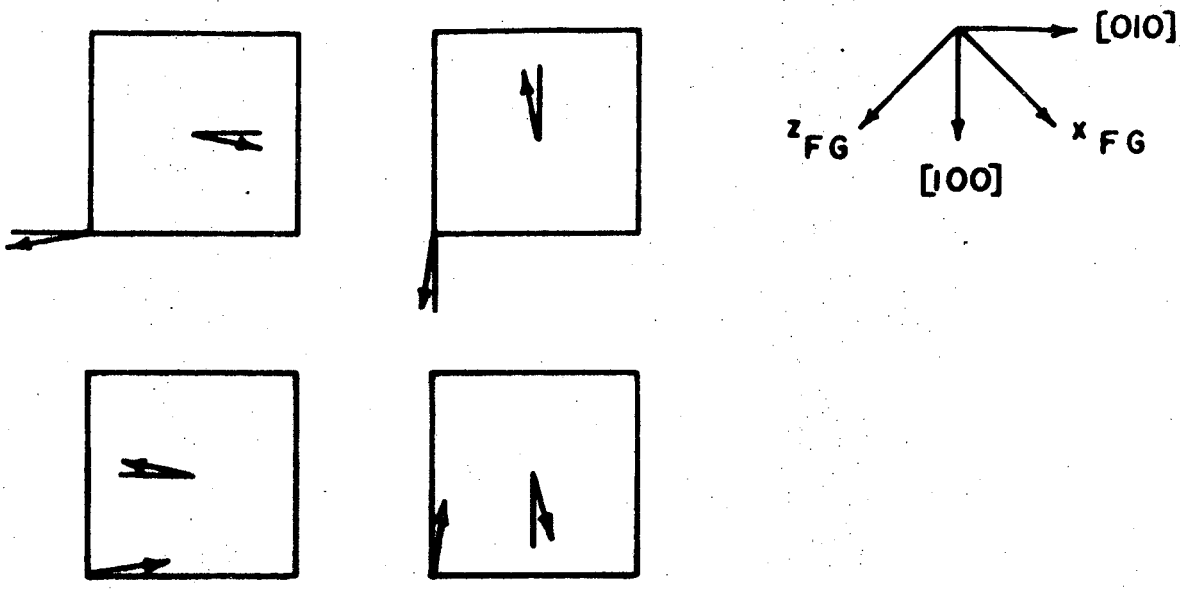

XBL 745-2996

Fig. 2

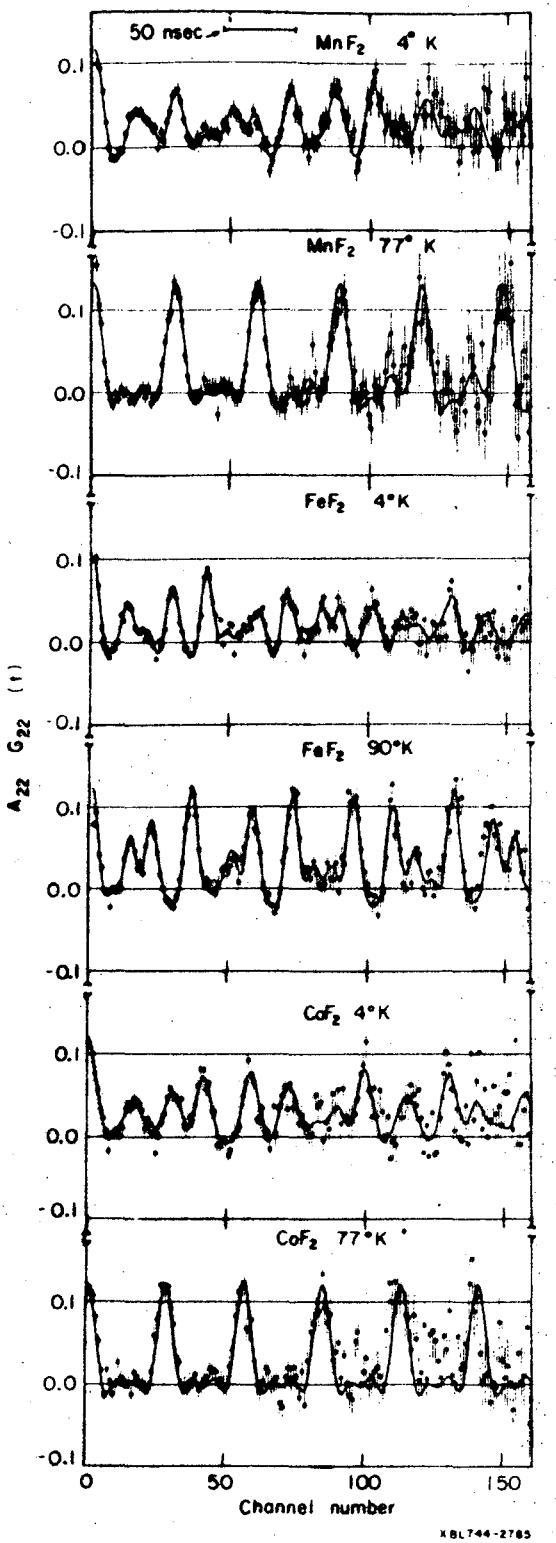
50 nsec
MnF2 4° K
MnF2 77° K
FeF2 4°K
FeF2 90°K
CoF2 4°K
CoF2 77°K
0.1
0.0
-0.1
A22 G22 (t)
0
50
100
150
Channel number
XBL744-2785

Fig. 3

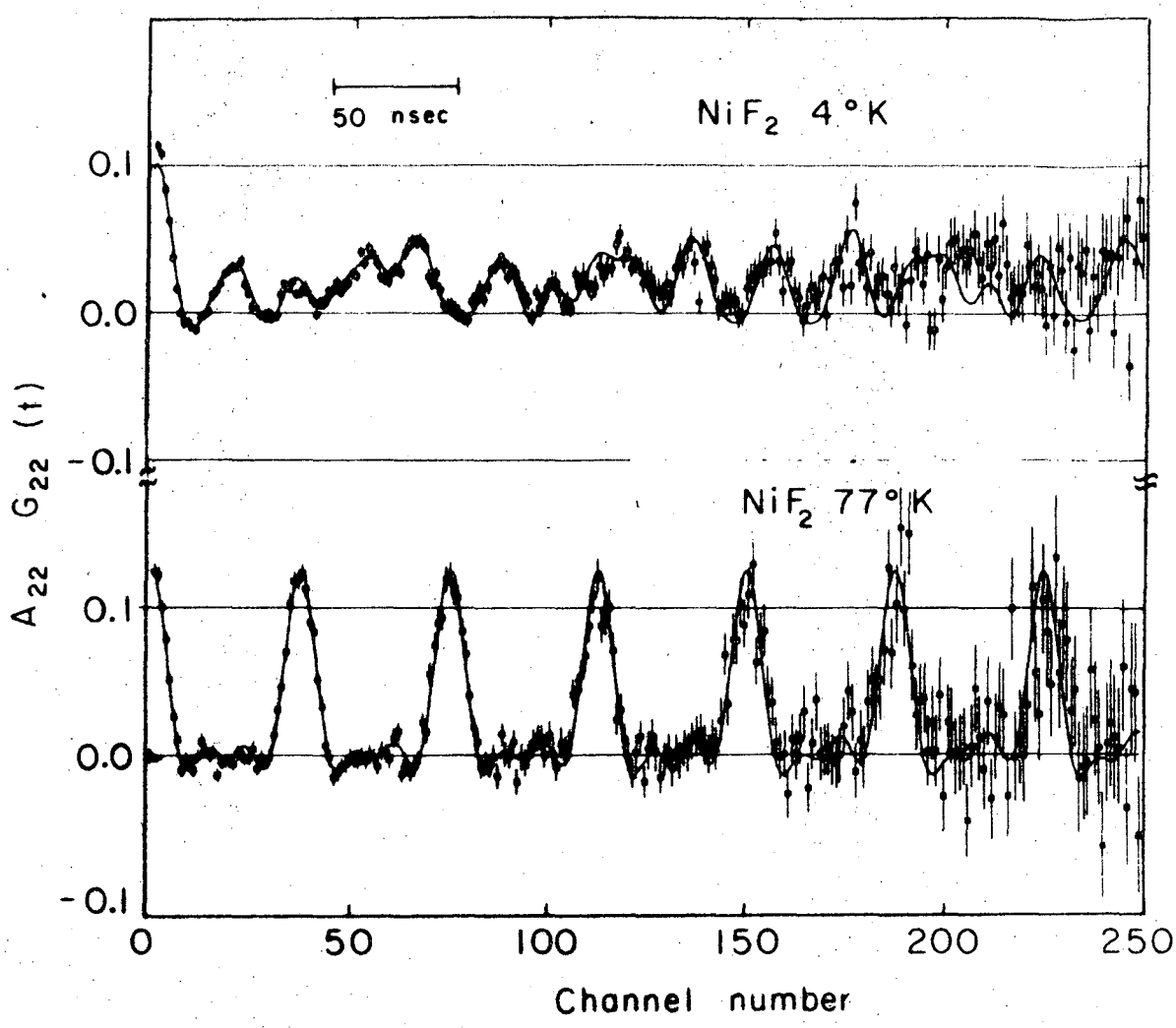
50 nsec
NiF2 4°K
NiF2 77°K
0.1
0.0
-0.1
A22 G22 (t)
0
50
100
150
200
250
Channel number
XBL745-2998

Fig. 4

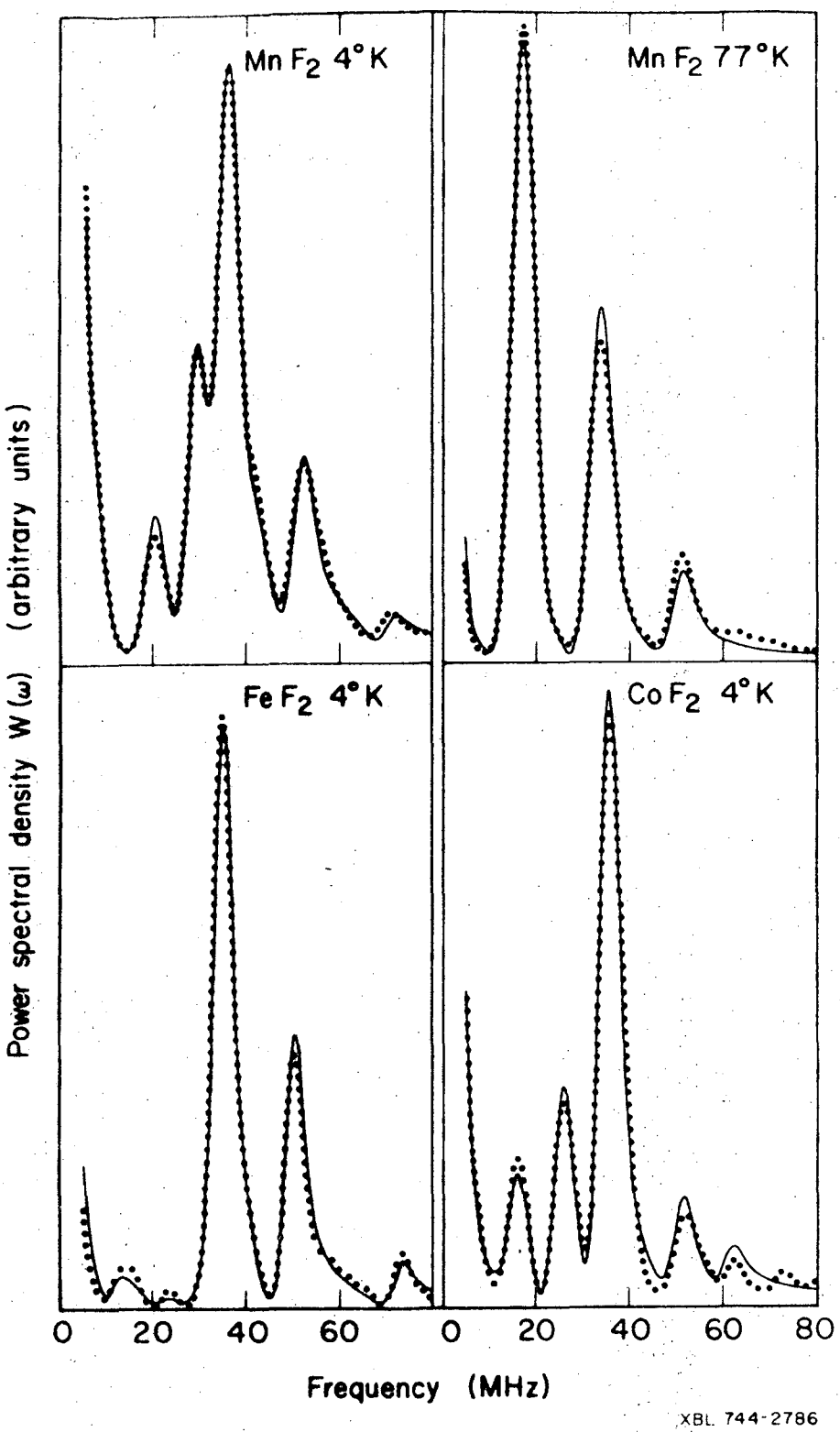
Mn F2 4°K
Mn F2 77°K
Fe F2 4°K
Co F2 4°K
Power spectral density W(ω) (arbitrary units)
0
20
40
60
0
20
40
60
80
Frequency (MHz)
XBL 744-2786

Fig. 5

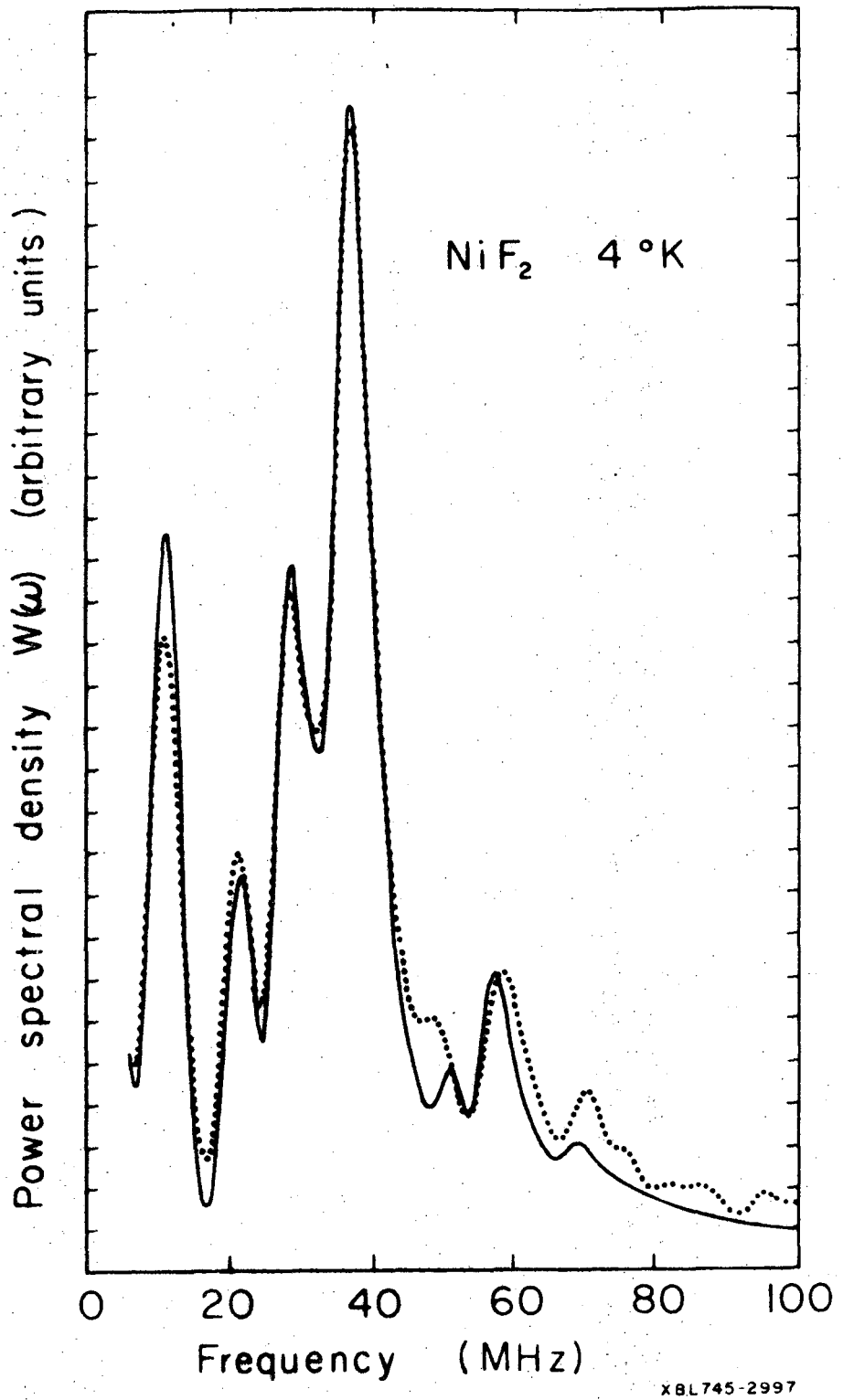
NiF2 4 °K
Power spectral density W(ω) (arbitrary units)
0
20
40
60
80
100
Frequency (MHz)
XBL745-2997

Fig. 6

TECHNICAL INFORMATION DIVISION
LAWRENCE BERKELEY LABORATORY
UNIVERSITY OF CALIFORNIA
BERKELEY, CALIFORNIA 94720